Pure Appl. Chem., Vol. 73, No. 5, pp. 771–783, 2001.

Phase diagrams at high temperature and high pressure. Determination and consequent developments*

M. Th. Cohen-Adad

Laboratoire des Matériaux Luminescents-UMR CNRS 5620, Université Claude Bernard-Lyon I, France

Abstract: This presentation focuses on condensed phases within the broader area of phase diagrams at high temperature and high pressure.

INTRODUCTION

One of the fields of concern to this conference is phase diagrams at high temperature and pressure. As the field covered by this topic is very large, this presentation will not be exhaustive and will be only focused on condensed phases.

The general condition of a two-phase equilibrium is described by Gibbs free energy relation $\Delta G = 0$ when composition, temperature, and pressure are the controlling parameters

$$d \ln \frac{a_i^{\alpha}}{a_i^{\beta}} = \frac{\Delta h_i^{\alpha \to \beta}}{RT^2} . dT - \frac{\Delta v_i^{\alpha \to \beta}}{RT} . dP$$

Under ambient conditions, the term $\Delta v_i/RT'$ related to pressure is small for condensed phases and can generally be neglected. It is not the case at high temperature where two problems arise due to the volatility of constituents and reactivity with the crucible.

High pressure is a good tool to prevent the volatility of constituents but it is also able to induce the formation of new phases.

MOTIVATIONS JUSTIFYING HIGH-TEMPERATURE AND HIGH-PRESSURE STUDIES

Practically, in most systems there are fields that cannot be described under ambient conditions. For example, phase equilibria are involved in the behavior of Earth and planet interiors. In particular, the successive chemical transformations of the minerals constituting Earth's mantle are related to the dependence of the temperature and pressure distribution [1] on the depth (Table 1).

Systems involving volatile constituents and particularly salt-water systems are implied in all hydrothermal processes.

The industrial applications of high temperature (and pressure) cover the production of special alloys, cements, ceramics, glasses, etc. and justify the extension of researches to these fields. For instance, a tensile strength as high as 25 000 kg/cm^2 is a required quality criterion for steel and the manufacture of nipples and valve bodies require steels working at 800–1000 atm [2].

However, the development of high-temperature and high-pressure studies requires the setting up of appropriate devices and the development of models agreeing with experiments which are able to

*Lecture presented at the 9th IUPAC International Symposium on Solubility Phenomena (9th ISSP), Hammamet, Tunisia, 25–28 July 2000. Other presentations are published in this issue, pp. 761–844.

Table 1 Chemical transformation of the minerals constituting Earth's mantle.

Layer of Earth's crust	Pressure, Gigapascals (GPa)	Temperature	Depth	Mineral
Lithosphere	upper limit, 1 GPa	600 °C		olivine $(Mg,Fe)_2SiO_4$ +
	lower limit, 3 GPa	1100 °C	100 km	pyroxenes $(Ca,Mg,Fe)_2Si_2O_6$ and $(Mg,Fe)SiO_3$ +
Upper mantle	up to 13 GPa	1400 °C	410 km	garnets $(Mg,Fe,Ca)_3Al_2Si_3O_{12}$ $(Mg,Fe)_2SiO_4$ β-phase γ-phase
Transition zone	up to 23 GPa	1600 °C	660 km	majorite $(Mg,Fe,Ca)_3(Al,Si)_2Si_3O_{12}$ perovskite $CaSiO_3$.
Lower mantle	up to 135 GPa	3500 ±50 °C	2900 km	perovskite $(Mg,Fe,Al)SiO_3$, $CaSiO_3$ and magnetowustite (Mg,Fe)O

describe the dynamics of compound formation and allow the extrapolation of results to domains out of the experimental range.

STATE OF THE ART

In practice,

- plasma furnaces allow one to reach temperatures between 5000 and 15 000 K,
- several hundred thousand degrees centigrade are obtained by means of a wire explosion,
- pressures between 1 and 10 TPa can be produced by shockwave techniques.

In routine laboratory experiments,

- the accessible pressures are between 1 and 170 Gpa
- temperatures are between 1000 and 5000 K.

HIGH-TEMPERATURE INVESTIGATIONS OF CRYSTALLIZATION CURVES IN SYSTEMS INVOLVING VOLATILE COMPONENTS

Influence of the volatility of constituents

The volatility of constituents changes the nominal composition of a sample and can induce an incorrect apparent retrograde solubility curve.

Systems involving volatile components must be investigated in closed vessels to prevent evaporation phenomenum. If the walls of the vessel are rigid, a dead volume must be left above the condensed phase to compensate the dilatation coefficients of sample and vessel, and, consequently, the volatile components will escape from condensed phase and will occupy the dead volume *V*.

The composition of sample must be corrected to take into account the loss of volatile component. The simple case of a binary salt-water system [3] can be proposed as an example of such a calculation.

The sample is characterized by

- its initial mass m_0 and
- its initial salt composition expressed in mole fraction x_0 or in mass per cent w_0.

Assuming that

- the vapor pressure of salt is negligible,
- salt is completely dissociated in liquid phase,
- the gas phase has a Van der Waals behavior,

the dead volume V can be calculated by an iterative method [3] when the ebullition curves of solutions (saturated or not) are determined under imposed pressures [3,4]. The mass of water in the gas phase is obtained by the relation $m_v = 18.V/v$ where v is the molar volume of pure water under the actual conditions of temperature and pressure and the global composition of condensed phases is deduced. It is given by:

$$w = \frac{w_0}{(1 - 18.\frac{V}{m_0}.\frac{1}{v})}$$

and depends on the ratio V/m_0. When this ratio tends to 0, w tends to w_0.

The increase of V/m_0 induces an apparent retrograde solubility curve as shown for the $CoCl_2$–H_2O system (Fig. 1a).

For a given initial composition w_0, thermal analysis investigations were performed for different values of V/m_0. Figure 1b shows such curves for w_0 = 40 g% of $CoCl_2$. Different breaks are observed, and the number of breaks varies with the value of the ratio. The temperature of these breaks are indicated on a vertical line passing through w_0.

- When $V/m_0 = 0$, only two breaks α and β are observed. They correspond respectively to the eutectic equilibrium ice-hexahydrate and to the limit of saturation in the hexahydrate.
- When the ratio is 10, α and β are still observed at the same temperature since the vapor pressure of the solution is very small. Anhydrous salt precipitates at higher temperature (point λ), The mass of precipitated salt increases with temperature increase, then decreases and a complete dissolution of cobalt chloride is observed at μ.
- For higher values of V/m_0, 100 for instance, α and β are obtained, then the crystallization of the dihydrate $CoCl_2.2H_20$ is observed at γ. This hydrate undergoes a peritectic decomposition into monohydrate at δ, this hydrate is peritectically decomposed into anhydrous salt at ε, and the mixture is completely melted at ν.

Similar investigations were repeated for different values of w_0. The results are given in Fig. 1a. The crystallization curves are only deformed when V/m_0 is small, but an apparent retrograde solubility curve appears for higher values of the ratio. Figure 2 presents the experimental distillation curves [3] drawn versus composition for different V/m_0 values. The crystallization curves are progressively deformed when the ratio V/m_0 increases.

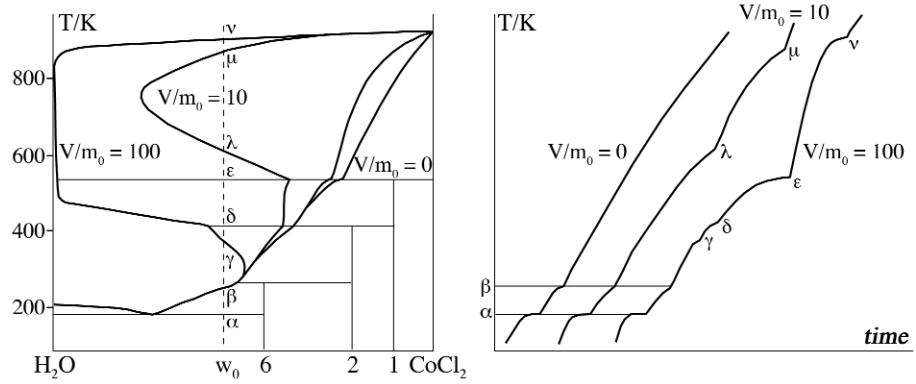

Fig. 1 Apparent crystallization curves in dependance on dead volume.

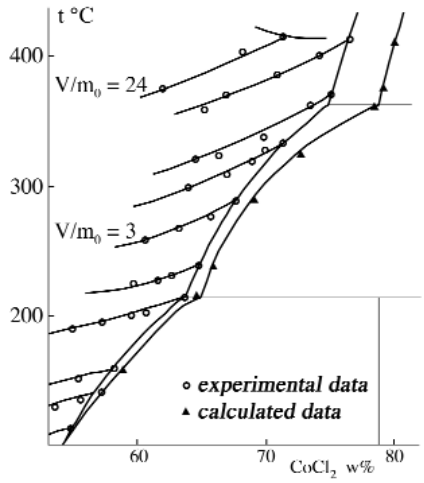

Fig. 2 Ebullition temperatures of $CoCl_2$ aqueous solutions vs. composition. Influence of dead volume.

Such an artefact of the crystallization curve can be prevented if:

- the composition of the sample is corrected, taking into account the loss of volatile component, as shown in Figs. 1 and 2 where the corrected crystallization curve is given, or
- the thermal analysis investigations are carried out without any dead volume.

Measurements without any dead volume

Figure 3a shows a device allowing one to perform thermal analysis measurements without a dead volume [5–8]. Figure 3b shows the measuring head.

The pressure is produced by a pneumatic jack *a* fed by nitrogen. The sample *b* is pressed through an inverted cup *c* (Fig. 3b) placed in a steel cylinder *d*. A piston *e* freely slides transmitting the pressure to the sample. Temperature is measured using thermocouple disk *f*. The measurement head is separat-

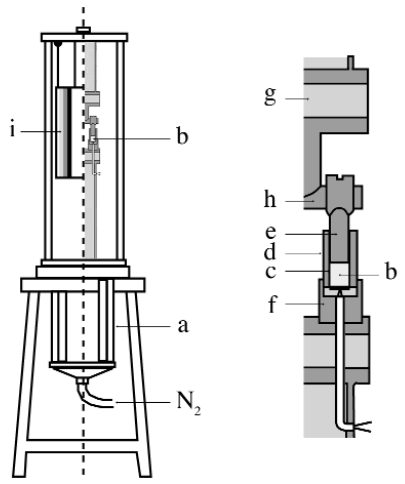

Fig. 3 DTA without dead volume: a) schematic view of device b) measurement head.

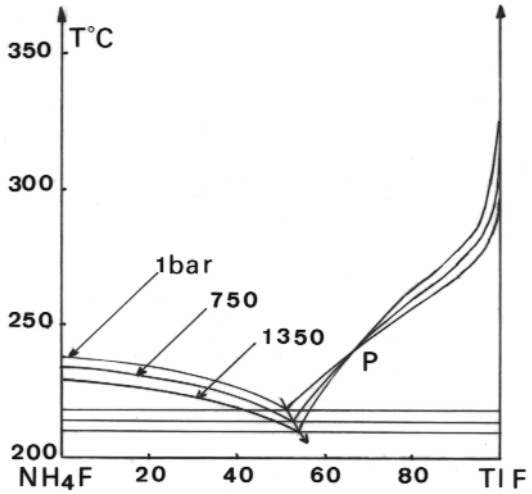

Fig. 4 Binary system NH_4F–TlF: Dependance on pressure.

ed from the pedestal by asbestos and mica disks *g*. Direct and differential measurements were performed. Two samples and a reference tube were used, and the pressure was equilibrated by the flask *h*. This first version was heated by an electric furnace I and could work up to 900 °C and 5 kbar.

A device based on the same principle was constructed by Saidi and Coffy. It could work up to 500 °C and 2 Gpa [10] and was used to investigate some isotherm and isobar isoplethic sections of the quaternary system SiO_2–Al_2O_3–M_2O–H_2O in order to prepare zeolitic aluminosilicates $M_{x/n}^{n+}(AlO_2)_x(SiO_2)_y$, mH_2O where *n* is the exchanging cation valency.

Several systems were investigated with this technique. The binary system NH_4F–TlF shown in Fig. 4 is one of them. It shows only an eutectic equilibrium which is shifted toward higher composition and lower temperature when the pressure increases. An invariant point P is observed on the crystallization curve of TlF. Furthermore, the increase in pressure allowed one to prevent the sublimation of NH_4F and observe the melting point which cannot be obtained under ambient pressure. The value corresponding to 1 bar was estimated from the extrapolation of the LnP = f(1/T) curve.

Occurrence of an invariant point

An invariant point is observed on the crystallization curve of a component if the conditions $dT = 0$ and $dx_1/dP = 0$ are satisfied for a value of the composition. The solid–liquid equilibrium law

$$-\frac{\Delta h_i^f}{T^2}.dT + \frac{\Delta v_i}{T}.dP + R.(\frac{\partial Ln\gamma_i x_i}{\partial x_i}).dx_i = 0$$

involves the transfer melting enthalpy Δh_i^f and the transfer melting volume Δv_i^f. Under isothermal conditions:

$$\frac{dx_i}{dP} = -\frac{\Delta v_i^f}{RT.(\frac{\partial Ln\gamma_i x_i}{\partial x_i})_{T,P}}$$

and this quantity is 0 if $\Delta v_i^f = 0$ [9]. This condition is observed for a stoichiometric compound if there is compensation between the volume changes due to the mixing $v_i^l - {}_i^{0,l}$ and to that due to the melting of the pure solid compound.

Shift of an equilibrium involving two solid compounds I (phase a), J (phase g), and a liquid (phase β)

The conditions $I^{\alpha} \Leftrightarrow I^{\beta}$ and $J^{\gamma} \Leftrightarrow J^{\beta}$ are related to

- the thermodynamical laws

$$-\frac{\Delta h_i^{\alpha\to\beta}}{T^2}.dT + \frac{\Delta v_i^{\alpha\to\beta}}{T}.dP + R.(\frac{\partial \ln \gamma_i x_i}{\partial x_i})_{T,P}.dx_i = 0$$

$$-\frac{\Delta h_j^{\gamma\to\beta}}{T^2}.dT + \frac{\Delta v_j^{\gamma\to\beta}}{T}.dP + R.(\frac{\partial \ln \gamma_j x_j}{\partial x_i})_{T,P}.dx_i = 0$$

- the Gibbs–Duhem relation applied to the β phase

$$x_i.\left(\frac{\partial \ln \gamma_i x_i}{\partial x_i}\right) + x_i.\left(\frac{\partial \ln \gamma_j x_j}{\partial x_j}\right)_{T,P} = 0$$

It follows that $$\frac{dT}{dP} = T.[\frac{x_i.\Delta v_i^{\alpha\to\beta} + x_j.\Delta v_j^{\gamma\to\beta}}{x_i.\Delta h_i^{\alpha\to\beta} + x_j.\Delta h_j^{\gamma\to\beta}}]$$

$$\frac{dx_i}{dP} = [\frac{x_j.\Delta h_j^{\gamma\to\beta}.\Delta h_i^{\alpha\to\beta}}{RT.(\frac{\partial \ln \gamma_i x_i}{\partial x_i})_{T,P}.[x_i.\Delta h_i^{\alpha\to\beta} + x_j.\Delta h_j^{\gamma\to\beta}]}].[\frac{\Delta v_i^{\alpha\to\beta}}{\Delta h_i^{\alpha\to\beta}} - \frac{\Delta v_j^{\gamma\to\beta}}{\Delta h_j^{\gamma\to\beta}}]$$

The stability condition $\frac{\partial \mu_i}{\partial x_i} \geq 0$ implies that $\frac{\partial \ln \gamma_i x_i}{\partial x_i} \geq 0$, the sign of $\frac{dx_i}{dP}$ depends on the sign of $[\frac{\Delta v_i^{\alpha\to\beta}}{\Delta h_i^{\alpha\to\beta}} - \frac{\Delta v_j^{\gamma\to\beta}}{\Delta h_j^{\gamma\to\beta}}]$ which can be positive or negative. Generally, it is negative when compound I is H_2O [9] and the three-phase equilibrium is shifted toward the increase of H_2O content when pressure increases. The NH_4F–TlF binary system presents the opposite case in which the increase of pressure induces a shift to increasing TlF content.

High-temperature phase diagram investigations

High-temperature phase diagrams investigations are difficult, arduous, expensive, and time-consuming.

⇒ The number of experiments must be limited and, for expensive components, it is important to reduce the size of samples.

At high temperature the reactivity with crucible is a big problem.

⇒ It is necessary to prevent such reactivity when possible.

Melting zone and floating zone techniques can be adapted in order to obtain the spectrum of a phase diagram. In particular, the floating zone technique is well adapted to prevent reaction with the crucible.

In these two techniques, a molten zone is created at the end of a feed rod and moves along the feed. During the movement, the feed melts progressively and a solid crystallizes behind the molten zone.

The spectrum of a phase diagram is obtained when a composition gradient is developed along the crystallized solid [11]. For this purpose, the feed rod is constituted by two parts A and B with different compositions C_A and C_B as shown in Fig. 5a. When the molten zone moves, there is a mutual solubility of A and B. During the moving, as the solubilized amounts of A and B are changed, the molten zone

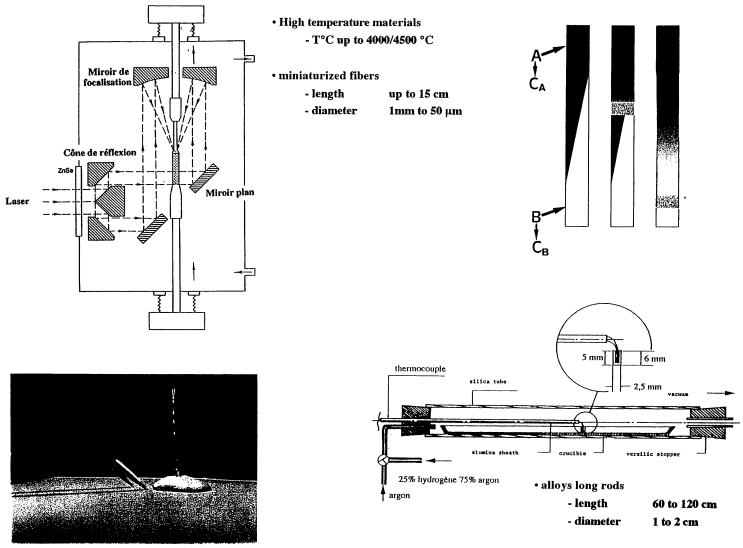

Fig. 5 Melting and floating zone techniques.

composition varies, inducing a progressive and continuous composition gradient along the crystallized rod. Such a procedure was applied to metallic and ceramics systems.

Long crystallized rods of alloys presenting an evolutive composition gradient were prepared using a classical horizontal melting zone device (Fig. 5b). The molten zone was created using an inductive heating, a thermocouple located inside the molten zone allows to follow the temperature. The composition gradient was developed on several centimeters (between 60 and 120 cm).

Due to the absence of a crucible, the floating zone is well adapted to prevent the risk of pollution in high refractory materials. A laser-heated pedestal growth (LHPG) device is presented in Fig. 5c. Two rods (feed and crystallized) are moved vertically. The molten zone, created by a focused laser beam, remains in equilibrium between the two rods due to the superficial tensions. Miniaturized crystallized fibers are obtained with this technique, and an example is presented in Fig. 5d.

Several binary and ternary systems were investigated using such a procedure [12,13]. The Al–Co binary system was one of them. It was investigated in totality by melting zone, but only the portion located between part A containing 16 at% of Co and part B consisting of pure Al is discussed herein. During the experiment, the molten zone composition progressively describes the liquidus curve between A and B. In this domain, the first crystallized solid is o-$Al_{13}Co_4$, which undergoes a peritectic decomposition into Al_9Co_2. When the Al content increases, the molten zone composition describes the liquidus of the crystallization field of Al_9Co_2 phase, which crystallizes up to the composition of eutectic where a co-crystallization of Al_9Co_2 and Al takes place. Then, the crystallization of pure Al is observed.

After a melting zone experiment, the crystallized rod was etched, polished, and analyzed by microprobe technique in order to identify the phases and by optical or electronic microscopy to examine the microstructure.

The results are presented in Fig. 6. The first micrographs present the typical microstructure of an uncomplete peritectic reaction. The core of grains is constituted by o-$Al_{13}Co_4$ corresponding to the primary crystallized phase. It is embedded into Al_9Co_2 formed by peritectic reaction. Between the grains, a crystallization of Al_9Co_2 needles inside an Al matrix corresponds to the crystallization of the remaining liquid. Then the Al_9Co_2 becomes the primary solid phase and when the molten zone composition

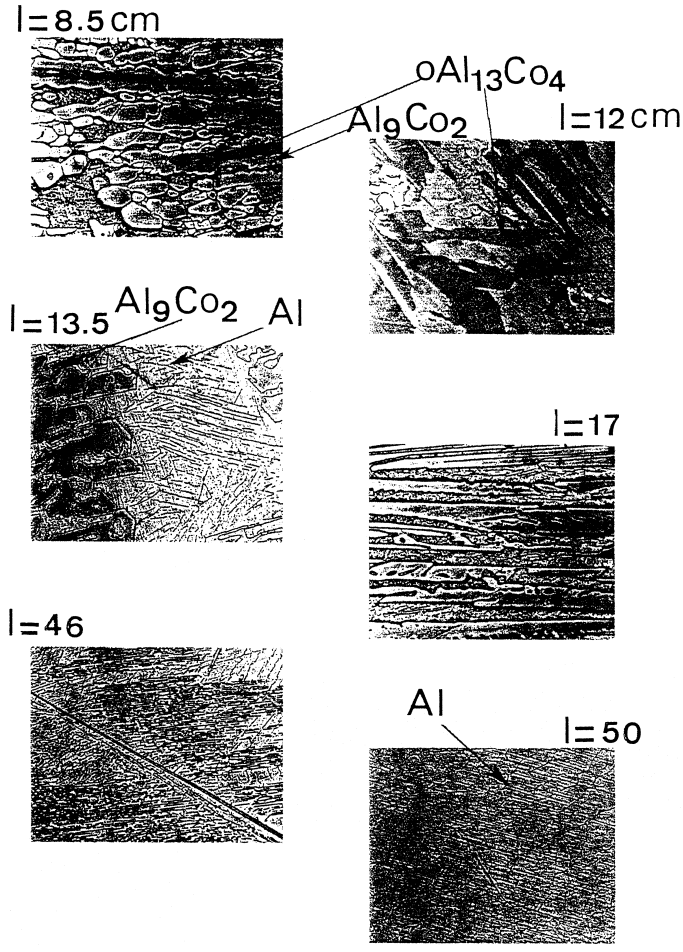

Fig. 6 Evolution of microstructure along the recrystallized rod.

reaches the eutctic point, the crystallized rod presents a characteristic eutectic microstructure. The end of the crystallized rod is constituted of pure aluminum grains, the eutectic microstructure being rejected at the boundaries of the grains.

This technique is fast and not expensive. A few samples are enough to draw a complete phase diagram spectrum even for complex systems. It presents also the possibility of linking phase composition and all physical properties able to be measured *in situ* along the crystallized rod (refractive index for optical materials, thermal conductivity, microhardness...). When the crystallized rod corresponds to a solid solution, this technique constitutes a combinatorial approach for discovering and optimizing materials [14].

ULTIMATE PRESSURE AND TEMPERATURE DEVELOPMENTS

Each range of pressure has its own specific features.

- Pressures below 50 kbar can be produced in piston cylinder apparatus (R. Cohen-Adad, A. Marchand, A. Tranquard, M. Rivière [5–8], M. Saïdi, G. Coffy [10]).

- Pressures above 50 kbar can be generated by apparatus developed by Bridgman [15], Balchan and Drickamer [16], Hall [17], Wilson [18], etc.
- For Mbar pressure, new types of apparatus (Vereschagin *et al*. [19], Kawai *et al*. [20], Mao and Bell [21], etc.) are required.

In practice, phase transformation up to melting can be followed up to 5000 K and/or 170 GPa using high-compression devices or diamond anvil cells.

Example of development obtained with high-compression apparatus

Different high-compression devices are described in the literature from those using pistons slanted on the conical face [16] to the high-compression belt [22] where the sample volume is 1 mm^3. Some of them have at least 180 kbar pressure capability [16,22].

The P-T diagram drawn up to 4000 K and 160 kbar and showing the direct transformation of hexagonal boron nitride to denser form [22] is an example of the studies performed with high-compression devices. The extension of the equilibrium line between the hexagonal and cubic forms [23] and the melting line of the hexagonal boron nitride as experimentally determined [24], the location of cubic-hexagonal-liquid triple point and the melting line of the cubic form result from this study and allow one to draw a good tentative phase diagram.

Diamond anvil cells

The Mbar diamond cell can be used for experiments under cryogenic conditions close to absolute zero and under high temperature up to 4000 K. A schematic view of the basic apparatus is given in Fig. 7a [25].

- The two diamond anvils are forced together using spring-loaded screws that rotate in opposition to advance the piston or by using a standard arm-lever block that applies more force than the advancing screws. The diamond anvils are cemented in place through a rigidly mounted sample gasket. The stress distribution must be such that the pressure on the compressed portion of the gasket is slightly higher than on the sample.
- For cryogenic experiments the cell is suspended in a liquid helium cryostat and, by utilizing an optical window in the crysostat, it is possible to perform IR, Raman, Mössbauer … spectra at low temperature.
- High temperatures can be achieved either with small resistive heaters surrounding the diamonds or by focusing a CO_2 or YAG laser beam on the sample. In this last case, temperatures up to 4000 K [1] can be reached at pressure up to 135 GPa. The focused spot is about 2 μm in size.
- Around the sample, the gasket hole is filled with a pressure-transmitting medium such as a soft liquid, solid or rare gas.
- Inside the gasket hole, small ruby chips are used for measuring pressure by excitation of their fluorescence [25].
- The vertical temperature gradients within the sample will be reduced if the pressure-transmitting medium is an insulator.

A complete model of the temperature distribution and the temperature-generated pressure field (sample + pressure-transmitting medium) was proposed by Gillet [27]. It gives the dependence on the heating power and enables the radial temperature gradient to be deduced.

The selective transparency of diamond from IR to X-ray and gamma-ray radiations permits *in situ* measurements during experiments (Fig. 7b). Some examples are presented to illustrate the scope of the device.

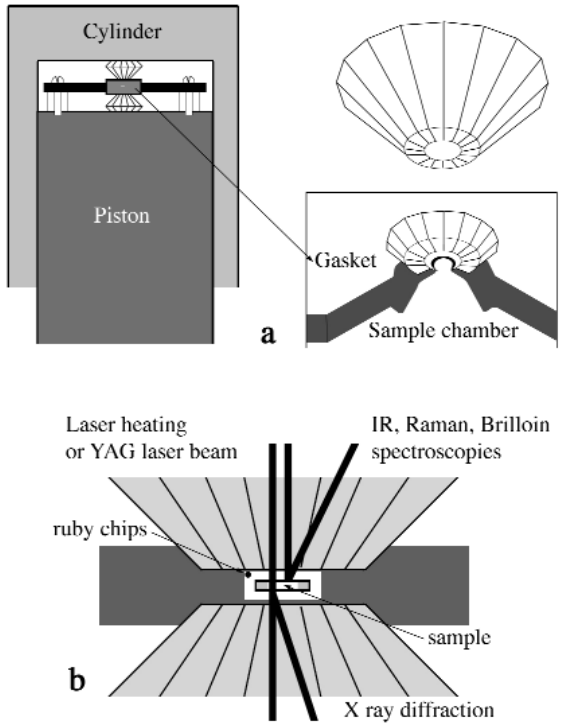

Fig. 7 Diamond anvil cells for cryogenic and high-temperature conditions.

In situ *study structural transformations of iron [28]*

Iron is the dominant constituent of the inner Earth's core, and informations on its behavior at high temperature and high pressure is important for the understanding of the physical properties of the earth such as observed seismic structure, chemical and dynamical coupling of the Earth's core and mantle, and the Earth's magnetic field.

In situ investigations were performed in a diamond anvil cell, and the structural change was followed using X-ray diffraction. Under high pressure and at room temperature, iron exists in an hexagonal compact symmetry (ε phase). During heating, the change of X-ray pattern indicates a structural change into a new orthorhombic β phase which can be also considered as a distortion of the Fcc γ phase induced by pressure.

Not only has this *in situ* study given evidence of a new phase but stability field of γ iron (between 32 and 40 GPa) and of the β phase (up to 100 GPa) was delimited.

Phases transitions followed by Raman spectroscopy combined with high temperature and pressure

Raman spectroscopy coupled with high temperature and pressure enables a direct experimental investigation of a material up to its melting point [26]. Together with IR, acoustic or neutron diffraction data, it leads to thermodynamical properties of compounds.

As an example, the quartz-coesite transition was monitored by *in situ* Raman spectroscopy under 7 GPa. A single crystal was progressively heated with a CO_2 laser in a diamond anvil cell [26]. The progressive heating was accompanied by a band broadening and a frequency shift toward high energy indi-

cating the partial transformation of quartz into coesite. The main important bands of quartz and coesite were present in the Raman spectrum of a sample quenched from high temperature. After laser heating, the polycrystalline area corresponding to the heated zone, consisted of a mixture of quartz and coesite.

Raman spectroscopy together with IR data were used to construct and substantiate models for heat capacity, vibrational entropy [26,29–40], and molecular volume. A formalism based on the vibrational Helmoltz free energy of a crystal, which included anharmonic correction [26], was applied to calcite. There was good agreement between the calculated and experimental points.

Shockwave techniques

Shockwave techniques are routinely used to study material properties at high pressure including material behavior both during and after shock compression. Some recent investigations showed that unexpected properties can be induced due to the attainable high pressure produced by such techniques.

These techniques require sophisticated instrumentation where the resulting one-dimension shockwave is detected. Measurement of wave and particle velocity behind the shock can be used to determine the final stress-volume state [41,42]. Conventional shockwave techniques employ:

- explosives;
- plate impact where pressure is directly liked to the velocity attainable by a flyer plate and where it is important to launch the projectile without distorting its flat front face and modifying its thermodynamic state during its accelaration; or
- energy deposition [41] using either high-power lasers developed for inertial-confinement-fusion research which can produce shock pressures far exceeding those possible by any previously employed laboratory techniques [41,43] or by irradiation with an intense pulsed relativistic electron beam [41,44].

Material response under dynamic compression must be studied for a wide variety of conditions. Continuous loading techniques [41,45,46] provide possibilities of identifying dynamic phase transitions in a single experiment and, in particular, can be used to the study short-lived phenomena such as occur during the passage of a shockwave.

CONCLUSIONS

This presentation was not exhaustive and, particularly, some important problems such as the behavior of organic materials, the biological effect of high pressure, the high-pressure safety, the solid-state physics of high temperature and pressure, and the theoretical aspect of dynamic pressure were either completely omitted or only approached.

The range of applications of high temperature and/or pressure is very large and covers:

- industrial production of alloys, cements, ceramics, and glasses that can be shaped;
- geo and planetary science where various properties of earth materials can be now studied and reproduced in laboratory experiments;
- immobilization of high-level nuclear waste elements in crystalline, dense bodies of minerals, and containment of spent nuclear fuel in monolithic canisters of a glass or a crystalline synthetic mineral, crystalline material being much more stable and having a much wider resistance against attack by water under pressure at elevated temperature.

Another interesting aspect of high pressure is that it tends to favor the formation of materials with an increase of coordination number of elements.

ACKNOWLEDGMENT

It is a pleasure to thank Prof. P Gillet for his help in the collection of high-pressure information used in this conference.

REFERENCES

1. P. Gillet. *C. R. Acad. Sci. Paris*, **320**, Serie IIa, 341 (1995).
2. D. S. Tsiklis. *Handbook of Techniques in High-pressure Research and Engineering*, Plenum Press, New York (1968).
3. M. Noailly. Thèse de 3ème cycle, Université de Lyon (1969).
4. B. Boinon. Thèse 3ème cycle, Université de Lyon (1969).
5. A. Marchand. Thèse Université de Lyon (1968).
6. R. Cohen-Adad, A. Marchand, A. Tranquard. *Bull. Soc. Chim.* **1**, 65 (1968).
7. R. Cohen-Adad, A. Marchand, A. Tranquard. *Acta Chimica*, Acad. Sc. Hongria **57**, 69 (1968).
8. M. Rivière. Thèse de 3ème cycle, Université de Lyon (1970).
9. I. Prigogine and R. Dufay. Thermodynamic chimique, edition Desoer Liege (1961).
10. M. Saidi and G. Coffy. *J. Therm. Anal.* **36**, 2635 (1990).
11. M. Th. Cohen-Adad, L. Laversenne, C. Goutaudier, G. Boulon. European patent May 2000, French patent June 2000.
12. M. Gharbi. Thèse 3ème cycle, Université de Lyon (1978).
13. M. Th. Cohen-Adad, M. Gharbi, C. Goutaudier, R. Cohen-Adad. *J. Alloys Comp.* **289**, 185 (1999).
14. M. Th. Cohen-Adad, L. Laversenne, C. Goutaudier, G. Boulon. European patent May 2000, French patent June 2000.
15. P. W. Bridgman. *Proc. Roy. Soc. A* **203**, 1 (1950).
16. A. S. Balchan and H. G. Drickamer. *Rev. Sci. Instr.* **32**, 308 (1961).
17. H. T. Hall. *Rev. Sci. Instr.* **31**, 125 (1960).
18. W. B. Wilson. *Rev. Sci. Instr.* **31**, 331 (1960).
19. L. F. Vereschagin, E. N. Yakovlev, G. N. Stepanov, K. Kh. Bibaev, B. V. Vinogradov, *Zh. Eksper. i Theor. Fiz. Pis'ma Red.* **16**, 240 (1972).
20. N. Kawai, S. Mochizuki, H. Fujita. *Phys. Lett.* **34A**, 107 (1971).
21. H. K. Mao and P. M. Bell. *Science* **191**, 851 (1976).
22. F. P. Bundy, R. H. Wentrop, Jr. *J. Chem. Phys.* **38**(5), 1144 (1963).
23. R. H. Wentorf, Jr. *Chem. Eng.* **68**, 177 (1961).
24. R. H. Wentorf, Jr. *J. Phys. Chem.* **63**, 1934 (1959).
25. H. K. Mao and P. M. Bell. In *High Pressure Science & Technology*, B. Vodar and Ph. Marteau (Eds.), Vol. 1, p. 15, Pergamon Press, New York (1980).
26. P. Gillet. *Phys. Chem. Miner.* **23**, 263 (1996).
27. A. Dewaele, G. Fiquet, P. Gillet. *Rev. Sci. Instr.* **69**(6), 2421 (1998).
28. D. Andrault, G. Fiquet, M. Kunz, F. Visocekas, D. Häusermann. *Science* **278**, 831 (1997).
29. M. Akaogi, N. L. Ross, P. F. McMillan, A. Navrotsky. *Ann. Mineral* **69**, 499 (1984).
30. A. Chopelas. *Phys. Chem. Miner.* **17**, 149 (1990).
31. A. Chopelas. *J. Geophys. Res.* **96**, 11817 (1991).
32. A. Chopelas, R. Boehler, T. Kao. *Phys. Chem. Miner.* **21**, 351 (1994).
33. P. Gillet, F. Guyot, G. D. Price, B. Tournerie, A. Le Cleac'h. *Phys. Chem. Miner.* **20**, 159 (1993).
34. A. M. Hofmeister. *Phys. Chem. Miner.* **14**, 499 (1987).
35. S. W. Kieffer. *Rev. Geophys. Space Phys.* **17**, 1 (1979).
36. S. W. Kieffer. *Rev. Geophys. Space Phys.* **17**, 20 (1979).
37. S. W. Kieffer. *Rev. Geophys. Space Phys.* **17**, 35 (1979).

38. S. W. Kieffer. *Rev. Geophys. Space Phys.* **18**, 862 (1980).
39. S. W. Kieffer. *Rev. Geophys. Space Phys.* **20**, 827 (1982).
40. E. Salje and K. Viswanathan. *Contrib. Miner. Petrol.* **55**, (1976).
41. J. R. Asay and L. C. Chhabildas. In *High Pressure Science & Technology*, B. Vodar and Ph. Marteau (Eds.), Vol. 2, p. 958, Pergamon Press, New York (1980).
42. R. G. McQueen, S. P. Marsj, J. W. Taylor, J. N. Fritz, W. J. Carter. In *High Velocity Impact Phenomena*, R. Kinslow (Ed.), Academic Press, New York (1970).
43. R. J. Traynor, N. C. Holms, R. M. More. In *High Pressure Science & Technology*, B. Vodar and Ph. Marteau (Eds.), Vol. 2, p. 965, Pergamon Press, New York (1980).
44. R. Billy-Salin. In *High Pressure Science & Technology*, B. Vodar and Ph. Marteau (Eds.), Vol. 2, p. 986, Pergamon Press, New York (1980).
45. F. Jamet. In *High Pressure Science & Technology*, B. Vodar and Ph. Marteau (Eds.), Vol. 2, p. 974, Pergamon Press, New York (1980).
46. Q. Johnson and A. C. Mitchell. *High Pressure Science & Technology*, B. Vodar and Ph. Marteau (Eds.), Vol. 2, p. 1977, Pergamon Press, New York (1980).